

**SOLAR CORONAL HEATING
AND THE
MAGNETIC FLUX CONTENT OF THE NETWORK**

D. A. Falconer,^{1,2} R. L. Moore,¹ J. G. Porter,¹ and D. H. Hathaway¹

Submitted to ApJ.
April 2003

1. Marshall Space Flight Center, SD 50/Space Science Department, Huntsville Al 35812
2. Physics Department, University of Alabama at Huntsville, Huntsville Al 35899

SOLAR CORONAL HEATING AND THE MAGNETIC FLUX CONTENT OF THE NETWORK

D. A. Falconer,¹ R. L. Moore, J. G. Porter, and D. H. Hathaway

Marshall Space Flight Center, SD 50/Space Science Department, Huntsville Al 35812

David.falconer@msfc.nasa.gov, ron.moore@nasa.gov, Jason.porter@nasa.gov,
David.H.Hathaway@nasa.gov

ABSTRACT

We investigate the heating of the quiet corona by measuring the increase of coronal luminosity with the amount of magnetic flux in the underlying network at solar minimum when there were no active regions on the face of the Sun. The coronal luminosity is measured from Fe IX/X-Fe XII pairs of coronal images from SOHO/EIT, under the assumption that practically all of the coronal luminosity in our quiet regions comes from plasma in the temperature range $0.9 \times 10^6 \text{ K} \leq T \leq 1.3 \times 10^6 \text{ K}$. The network magnetic flux content is measured from SOHO/MDI magnetograms. We find that the luminosity of the corona in our quiet regions increases roughly in proportion to the square root of the magnetic flux content of the network and roughly in proportion to the length of the perimeter of the network magnetic flux clumps. From (1) this result, (2) other observations of many fine-scale explosive events at the edges of network flux clumps, and (3) a demonstration that it is energetically feasible for the heating of the corona in quiet regions to be driven by explosions of granule-sized sheared-core magnetic bipoles embedded in the edges of network flux clumps, we infer that in quiet regions that are not influenced by active regions the corona is mainly heated by such magnetic activity in the edges of the network flux clumps. Our observational results together with our feasibility analysis allow us to predict that (1) at the edges of the network flux clumps there are many transient sheared-core bipoles of the size and lifetime of granules and having transverse field strengths $> \sim 100 \text{ G}$, (2) ~ 30 of these bipoles are present per supergranule, and (3) most spicules are produced by explosions of these bipoles.

Subject headings: Sun: corona – Sun: magnetic fields – Sun: UV radiation

¹ Physics Department, University of Alabama at Huntsville, Huntsville Al 35899

1. INTRODUCTION

The Sun's outer atmosphere, the corona, glows in EUV and soft X-ray emission and extends beyond the planets as the solar wind. This remarkable performance is basically due to the high temperature of the corona near the Sun (Parker 1963, 1987; Withbroe 1992). From roughly $0.01 R_{\text{Sun}}$ above the photosphere out to distances of $1 R_{\text{Sun}}$ or more, the average temperature is above 10^6 K (Withbroe 1988; Foley et al 1996; Cranmer 2002). Consequently, the coronal plasma preferentially emits EUV and soft X-ray photons ($h\nu \sim kT \sim 0.1$ keV, $\lambda \sim 100$ Å), the density scale height in the inner corona is $\sim 0.1 R_{\text{Sun}}$, and the outer corona stretches into the solar wind. Thus, the corona owes its existence and character to heating that keeps it hundreds of times hotter than the photosphere. This much has been understood for decades, but the heating process still eludes us. So, coronal heating remains a premier problem in solar physics, one of broad importance to astrophysics and of key importance to heliospheric physics and space weather.

The energy consumed in coronal heating comes from the interior of the Sun. This energy is very likely a by-product of the outflow of heat through the convection zone: the convection zone acts as a heat engine, converting some of the thermal energy into mechanical and magnetic energy, some of which enters the corona and dissipates into heat. While it is nearly certain that coronal heating conforms to this general framework, the specifics of the actual heating process – the dominant modes and mechanisms of the magnetomechanical energy generation, transport, and dissipation – remain obscure.

From coronal images and their comparison with photospheric magnetograms, it is clear that magnetic field is directly involved in coronal heating all over the Sun (Withbroe & Noyes 1977; Vaiana & Rosner 1978). The corona out to a few R_{Sun} is obviously a magnetic formation (e.g., Sheeley 1992). Everywhere on the Sun there is enough magnetic flux in the photosphere that the overlying corona is filled with magnetic field strong enough to show itself in coronal structure on all scales, from short loops and narrow plumes rooted in the lanes of the magnetic network ($< \sim 10,000$ km across), to larger loops in and between active regions ($\sim 0.1 - 1 R_{\text{Sun}}$ long), to the largest streamers and coronal holes ($> \sim 1 R_{\text{Sun}}$ in lateral extent) (Acton et al 1992; Acton 1996; Falconer et al 1997, 1998; Porter, Falconer & Moore 1998; Schrijver et al 1999). Simply because the corona is permeated with magnetic field strong enough to confine or direct the coronal plasma, the field is perforce a factor in the heating process.

Moreover, comparison of coronal images and photospheric magnetograms indicates that most coronal heating is a consequence of the magnetic field: the corona is more luminous in EUV and X-ray emission, and hence there is more heating, when and where there is more magnetic flux. Over the 11-year cycle of solar magnetic activity, the yearly-average luminosity of the corona waxes and wanes in step with the total magnetic flux on the Sun, the X-ray luminosity changing by roughly a factor of 10 as the total magnetic flux changes by a factor of 5 (Pevtsov & Acton 2001). The greatest concentrations of magnetic flux found on the Sun are active regions with sunspots, and these stand out as the brightest regions in coronal images (except briefly during some flares in spotless regions). In a decayed active region that has lost its spots, the magnetic flux is less concentrated than in active regions with spots and the coronal emission is dimmer, but still brighter than in quiet regions, comparable areas of which contain yet less magnetic flux (for example, see Figure 1 of Falconer et al 1997). Thus, it appears that among regions of roughly the same size, coronal heating increases with magnetic flux content, and hence that the magnetic field is active in the heating process. Close inspection of the magnetic setting of the brighter coronal loops rooted in active regions shows that most are rooted near polarity inversion lines along which the magnetic field is strongly sheared and productive of

frequent microflares (Falconer et al 1997, 2000; Porter et al 1998). This, along with the profusion of polarity inversion lines and microflaring in the magnetic network, further suggests that coronal heating in any region of the Sun is driven by fine-scale magnetic activity in that region, be it an active region, a quiet region, or a coronal hole (Parker 1983, 1991; Porter et al 1987; Porter & Moore 1988; Porter, Fontenla, & Simnett 1995; Falconer et al 1998; Moore et al 1991, 1999).

The above correspondences between coronal brightness and magnetic flux, while only qualitative or loosely quantitative, do establish that coronal heating generally does increase with magnetic flux in some manner. This is enough to suggest that a more quantitative knowledge and analysis of this scaling, more tightly specifying the dependence of the heating on magnetic flux, might clarify the heating process.

The energy flux required for coronal heating in active regions ($\sim 10^7$ erg cm⁻² s⁻¹) is roughly 20 times that for sustaining the corona and solar wind in quiet regions and coronal holes (Withbroe & Noyes 1977; Withbroe 1988). On the other hand, even during solar maximum, active regions seldom if ever cover as much as 10% of the Sun's surface (Allen 1973; Harvey-Angle 1993). Hence, throughout the solar cycle, the total heating of the corona elsewhere than in active regions is comparable to or exceeds that in active regions. In addition, most of the solar wind comes from the extension of the corona rooted in coronal holes and quiet regions, not from active regions (Withbroe 1992). In these respects, the heating of the corona outside of active regions is as important or more important than the coronal heating in active regions.

The magnetic field that fills the body of the corona in quiet regions is mainly rooted in the magnetic network, the aggregate of flux clumps distributed along the edges of the supergranule convection cells (e.g., Leighton 1963; Dowdy, Rabin, & Moore 1986; Moore et al 1999). This basic magnetic linkage motivates our approach in the present work: we investigate coronal heating by examining the dependence of the luminosity of the corona in quiet regions on the magnetic flux content of the underlying network. In contrast to active regions and their remnants, in and among quiet regions devoid of noticeable remnants of old active regions it is not obvious from visual comparison of magnetograms and coronal images (such as in Figure 1 of Falconer et al 1997) whether there is any correlation at all between coronal luminosity and the amount of magnetic flux in the network. Although we would have been surprised to not find some discernible positive correlation from careful measurement of the luminosity and flux, at the outset of the work reported here, to our knowledge, the question remained open even at this primitive level.

We have measured the coronal luminosity and network magnetic flux in a few large quiet regions that were observed during solar minimum and that had well-mixed and nearly equal amounts of opposite-polarity flux. We find that the luminosity increases roughly as the square root of the magnetic flux. If coronal heating in quiet regions is driven by fine-scale activity in the network, the square-root scaling suggests that this activity is located mainly at the edges of the network flux clumps.

2. DATA AND DATA REDUCTION

In this study, for each of four consecutive days (1996 December 27-30) during the minimum phase of the solar cycle, we analyzed the structure and luminosity of the corona in a large square of quiet region, $0.5 R_{\text{Sun}}$ wide, centered on the face of the Sun, as in Figure 1. For each day, the coronal data are from a pair of coronal EUV images taken within half an hour of each other by the Extreme-Ultraviolet Imaging Telescope (EIT) (Delaboudinier et al 1995) of the Solar and

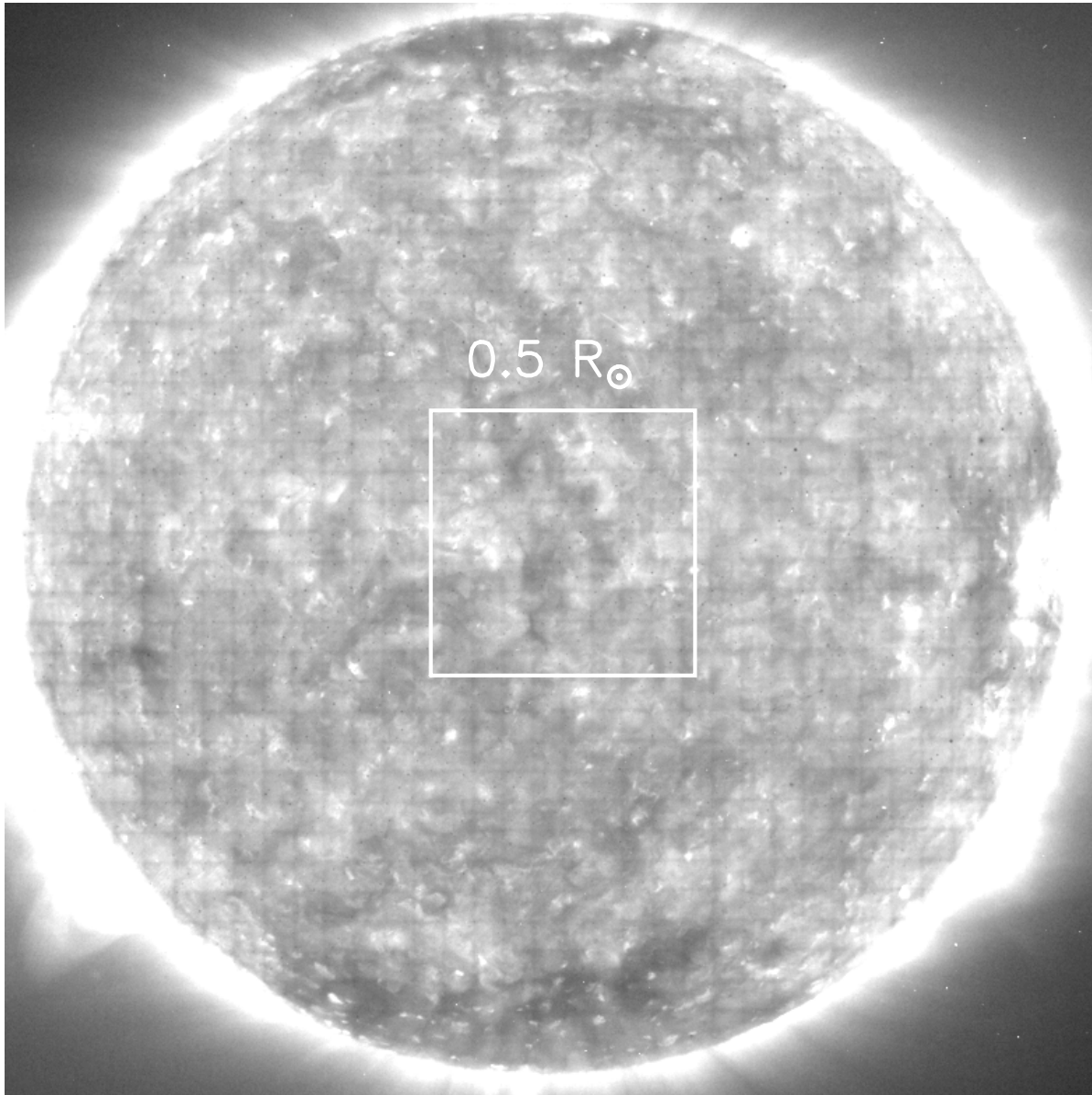


Figure 1 EIT Fe IX/X image of the quiet corona on 1996 December 28, when there were no active regions on the face of the Sun. The white square is centered on the Sun, and is $0.5 R_{\text{Sun}}$ wide. Solar north is up, and west is right.

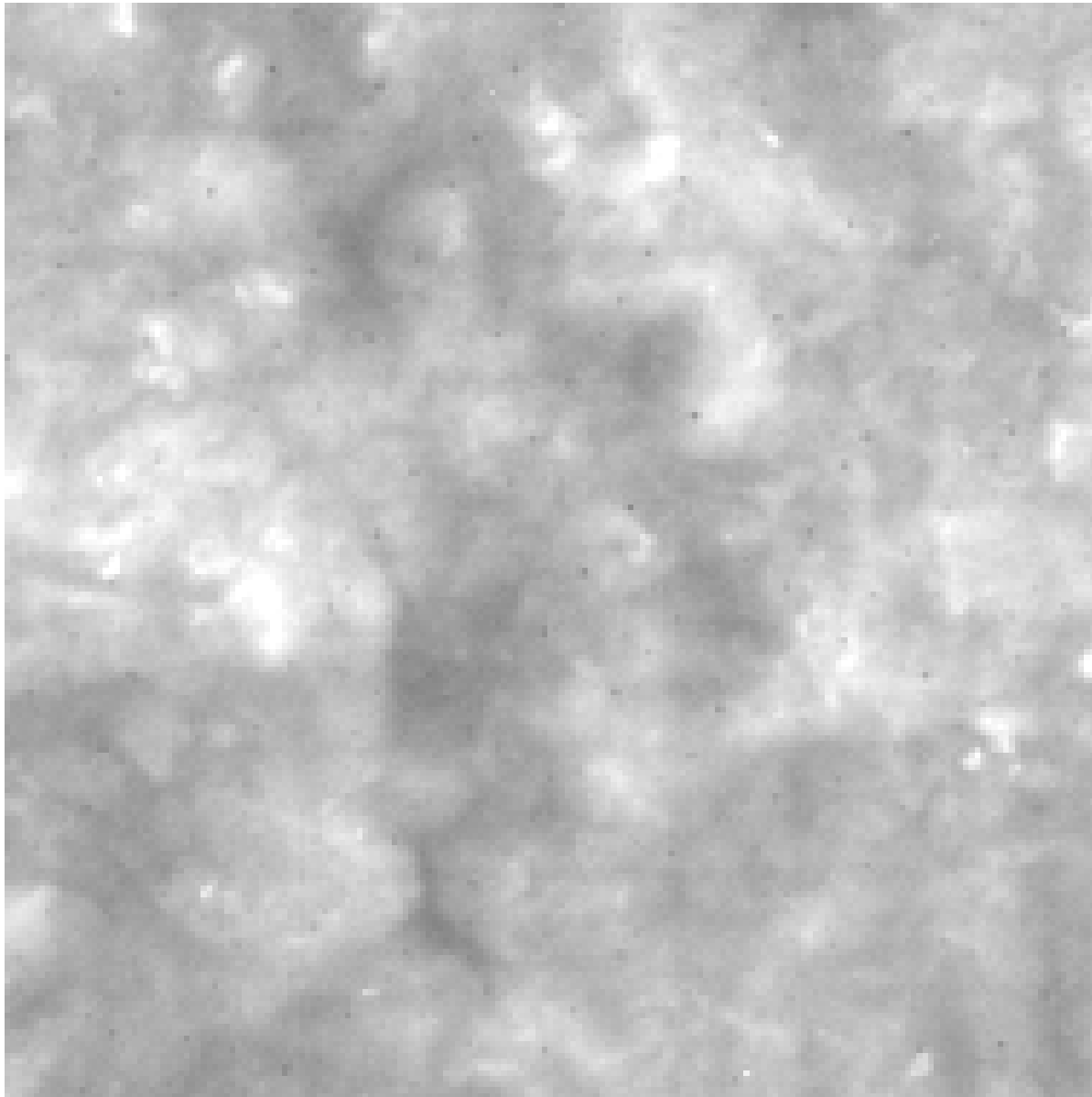
Date (Dec 1996)	EIT Fe IX/X Image (UT)	EIT Fe XII Image (UT)	MDI Magnetogram (UT)
27	17:18	17:43	16:03
28	19:24	19:37	16:03
29	19:00	19:03	16:03
30	19:29	19:39	16:03

the other is an Fe XII 195 Å filtergram. The dates and times of the eight coronal images used are listed in Table 1. The EIT images are composed of square pixels, each 2.6 arcsec wide.

By solar rotation, the heliographic region subtended by our $0.5 R_{\text{Sun}}$ central square at any given time passes entirely out of this box in a little less than three days. This and physical evolution made the structure of the corona in the central square different in detail on each of our four days. However, on all four days the corona in the central square appeared to be essentially the same as in Figure 1, in character of structure and average brightness.

The Fe IX/X image in Figure 2 is an enlargement of the central square of Figure 1. This image shows brightness spatial variations from as small as a single pixel ($\approx 2,000$ km) to larger than the span of a few supergranules ($\geq 100,000$ km). In quiet regions like this, the total coronal image can be deconvolved into two components by spatial filtering: a small-scale component comprised of the structure that is smaller than about 10,000 km (that is, smaller than roughly the width of the lanes of the magnetic network), and the large-scale remainder comprised of the structure that is larger than about 10,000 km. Adhering to our previous work (Falconer et al 1998), on which the present work builds, we call these two complements of the quiet-region corona the *coronal network* and the *large-scale corona*. As was shown in Falconer et al (1998), the coronal network stands on, and bushes out from, the network of magnetic flux clumps observed in photospheric magnetograms. The observed scale and structure of the coronal network indicates, in agreement with the mixed-polarity nature of the network, that the coronal network is the coronal-temperature ($T \sim 10^6$ K) component of the magnetic network and mostly resides at heights below about 10,000 km, much of it in closed magnetic loops within the network (Falconer et al 1998). In contrast, the large-scale corona is the main body of the quiet-region corona; it is also rooted in the magnetic network but extends much higher than the coronal network (e.g., see Dowdy et al 1986).

The spatial filtering technique that we have devised to filter out the coronal network and leave the large-scale corona is one that we call a triple-pass, peak-clipping, picture-frame filter. The shape and size of the filter window is shown in Figure 2. The averaging window is a square with a smaller central square blocked out. The outer square is about two-thirds of a network cell wide (11 pixels or 21,000 km), and the central blocking square is about one-third of a network cell wide (5 pixels or 9,000 km). The average brightness of the coronal image in this picture-frame window is approximately the brightness that the large-scale corona contributes to the total brightness of the pixel on which the window is centered. Replacing the brightness of each pixel of the original image with the average brightness in its picture-frame window yields a first-approximation image of the large-scale corona. This first approximation contains artifacts produced by this first pass of the picture-frame filter: the smoothed image has a faint bright feature the size and shape of the picture-frame filter centered on each pixel that is outstandingly bright in the original image. We remove these artifacts by repeating the smoothing operation two more times, once on each of two progressively “clipped” versions of the original image. First, the brightness of each brighter pixel in the original image (that is, the brightness of each pixel that is more than 30% brighter in the original image than in the first-pass smoothed image) is clipped to be only 30% brighter than in the first-pass smoothed image. Then this first clipped image is smoothed to produce a second-pass smoothed image. This second smoothed image is then used together with the original image to produce a second clipped image, in which no pixel is more than 30% brighter than the brightness of that pixel in the second-pass smoothed image. Finally, this second clipped image is smoothed by a third pass of the picture-frame filter. In



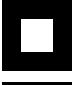
Picture-Frame
Filter:  | 10^4km
 $2 \times 10^4\text{km}$

Figure 2 Enlargement of the image of the Fe IX/X quiet corona in the central square of Figure 1. The size and shape of our picture-frame spatial filter are shown below the image.

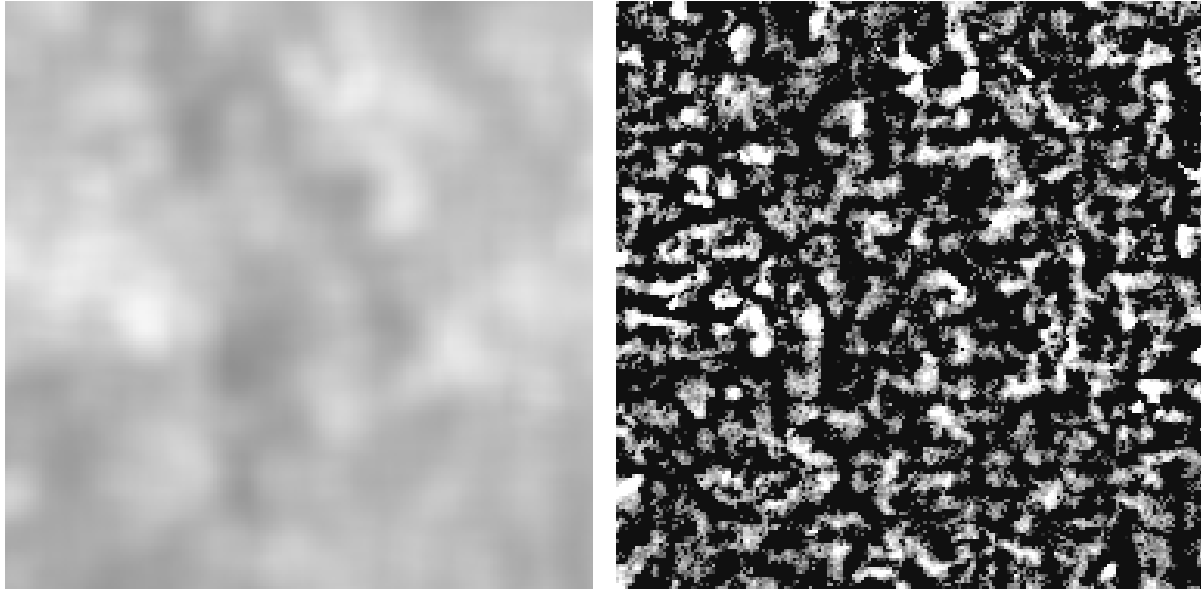


Figure 3 The two complementary spatial components comprising the coronal image of Figure 2. Left: The large-scale corona. Right: The coronal network. In each panel, the brightness is scaled to the brighter pixels in that image. In absolute intensity, the average brightness of the large-scale corona is about 20 times that of the coronal network.

practice, the third-pass smoothed image shows no noticeable artifacts and so is an adequately pure image of the large-scale corona.

The first panel of Figure 3 is the image of the large-scale corona obtained from our spatial filtering of the total-corona image in Figure 2. The second panel of Figure 3 is the image of the coronal network obtained by subtracting the image of the large-scale corona from the image of the total corona. From Falconer et al (1998), we know that only about 5% of the total coronal emission from quiet regions like that in Figure 2 is emitted by the coronal network; the rest comes from the large-scale corona. This is why the coronal network is seen only faintly and indistinctly in images of the total corona.

Because the coronal network is the coronal-temperature component of the magnetic network, it is plausible that this plasma is heated mainly by in situ magnetic activity (Falconer et al 1998). If so, we would expect its coronal luminosity to have an appreciable positive dependence on the magnetic flux content of the network. The objective of this paper is to investigate the heating of the extended body of the quiet corona, which may be qualitatively different than the heating of the much lower lying coronal network. We think that the coronal network and the large-scale corona may be heated in different ways because it is our view that the two components are more or less magnetically disparate, in the manner proposed by Dowdy, Rabin, & Moore (1986). That is, from the structure and magnetic setting of the coronal network, it appears that much of the coronal network plasma resides in magnetic loops that have lengths and heights of $\sim 10,000$ km and less, while the body of the quiet corona resides in much higher- and farther-reaching magnetic loops and funnels (Falconer et al 1998). To investigate the heating of the large-scale corona alone we examine the dependence of the luminosity of the large-scale corona on the magnetic flux content of the network, instead of examining the dependence of the luminosity of the total corona on the network flux content. Even though the

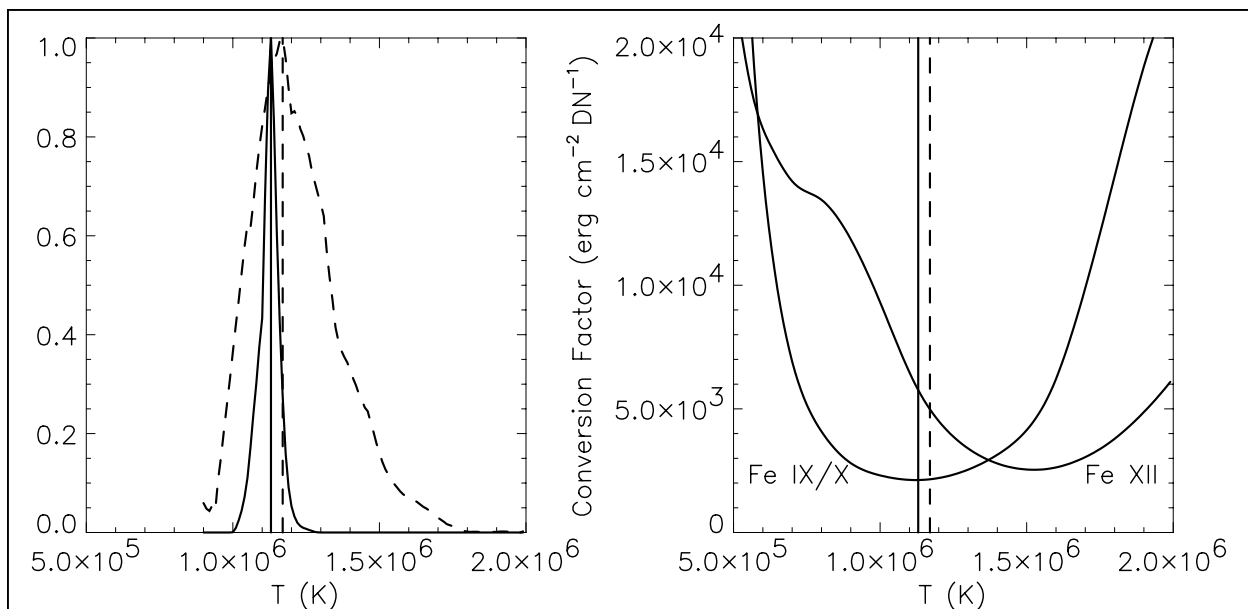


Figure 4 The basis of our choice of the Fe IX/X images rather than the Fe XII images for obtaining coronal luminosity from image brightness. **Left:** Filter-ratio temperature histograms (solid curve for the large-scale corona, dashed curve for the coronal network) with their peak temperatures marked by the corresponding vertical lines. **Right:** Temperature dependence of the conversion factor for obtaining luminosity from image intensity for isothermal coronal plasma viewed by EIT through its Fe IX/X filter (left curve) or through its Fe XII filter (right curve). The two vertical lines mark the histogram peak temperatures for the large-scale corona (solid line) and the coronal network (dashed line).

contribution of the coronal network to the total coronal luminosity is small, we remove it because we think that it would give a bias toward a more positive dependence.

From the co-registered EIT Fe IX/X-Fe XII image pair for each day, we obtain the rate of energy loss by radiation, separately for the large-scale corona and for the coronal network. In the approximation that the coronal plasma in any pixel is isothermal, the brightness ratio of the pair of images of the large-scale corona in a pixel and the brightness of the Fe IX/X large-scale corona in that pixel together, via the CHIANTI code (Dere et al 1997), give the temperature and emission measure of the large-scale corona in that pixel. The temperature and emission measure in a pixel, via the radiation loss function of Cook et al (1989), give the radiation flux emitted by the large-scale corona in that pixel. In this way, the temperature, emission measure, and radiation flux of the coronal network were also computed for each pixel of an image pair.

The filter-ratio temperature of the large-scale corona was nearly constant throughout the central square and was nearly the same on all four days. For the four days combined (a total of 10^5 pixel temperatures) the filter-ratio temperature histogram for the large-scale corona is shown in the first panel of Figure 4. This histogram narrowly peaks slightly above 1.1×10^6 K; it has a half-maximum full width of about 0.05×10^6 K. A temperature near 1.1×10^6 K is reasonable for the corona in very quiet regions such as ours: Withbroe & Noyes (1977) give a temperature range of $(1.1-1.6) \times 10^6$ K for the large-scale corona in quiet regions. While the histogram peak temperature is probably near the average temperature of the plasma in the large-scale corona in our quiet regions, we expect that the temperature range of this plasma is considerably greater than the width of the histogram. Imaged EUV spectra of an isolated coronal loop in an active region have shown the true temperature range along the length of the loop to be several times

Table 2. Average Fluxes of Coronal Radiation and Network Magnetic Field in our Quiet Regions			
Date (Dec 1996)	Large-Scale Corona Radiation Flux ($\text{erg cm}^{-2} \text{s}^{-1}$)	Coronal Network Radiation Flux ($\text{erg cm}^{-2} \text{s}^{-1}$)	Network Magnetic Flux (Gauss)
27	1.1×10^5	$\sim 4 \times 10^3$	2.0
28	1.1×10^5	$\sim 4 \times 10^3$	2.3
29	1.1×10^5	$\sim 4 \times 10^3$	2.2
30	1.1×10^5	$\sim 4 \times 10^3$	2.3
Average:	1.1×10^5	$\sim 4 \times 10^3$	2.2

larger than that given by the filter-ratio method that we use (Schmelz et al 2001; Martens, Certain, & Schmelz 2002; Schmelz 2002). For our quiet regions, we expect that the temperature range in the large-scale corona was much narrower than in an active-region loop, but still substantially wider than the width of our temperature histogram. Specifically, we assume that the bulk of the plasma in the large-scale corona was in the temperature range $(0.9-1.3) \times 10^6$ K.

For the ideal case of isothermal coronal plasma, the CHIANTI code can be used to compute the ratio (conversion factor) between the brightness of an EIT image pixel and the spectrum-integrated coronal radiation flux (i.e., the coronal luminosity per unit area). The two curves in the second panel of Figure 4, one for the Fe IX/X filter and the other for the Fe XII filter, give this conversion factor as a function of the temperature of the isothermal plasma. The Fe IX/X curve shows that the EIT Fe IX/X images are most sensitive to emission from coronal plasma at temperatures around 1.1×10^6 K, and that the conversion factor is nearly constant (within a few tens of percent) for temperature in the range $\pm 0.2 \times 10^6$ K centered on 1.1×10^6 K. Hence, if, as we assume, the temperature of practically all of the plasma in the large-scale corona in our quiet regions was in this range, the spatial brightness variations seen in our Fe IX/X images of the large-scale corona are closely proportional to corresponding variations in the luminosity of that component of the corona. The scaling that we find between the luminosity of the large-scale corona and the network magnetic flux does rest on the validity of our assumed temperature range of the large-scale corona. For the large-scale corona in very quiet regions such as ours, we think that this assumption is probably a good approximation, but this remains to be ascertained by sensitive EUV imaged spectra such as are expected from the forthcoming Japan/US/UK Solar-B mission.

The two conversion-factor curves in Figure 4 show that in our temperature range around 1.1×10^6 K the ratio of image brightness to luminosity depends much more strongly on temperature in the EIT Fe XII images than it does in EIT Fe IX/X images. For this reason, we used the Fe IX/X images rather than the Fe XII images to obtain coronal luminosity from image brightness, and throughout this paper we show Fe IX/X images rather than Fe XII images. In Figure 4 (first panel), the temperature histogram for the coronal network in our quiet regions peaks near the peak of the histogram for the large-scale corona, but is much broader, having a half-maximum full width of about 0.3×10^6 K. While we recognize that our assumption of nearly all of the coronal plasma having temperature in the range $(0.9-1.3) \times 10^6$ K is only a rough approximation for the coronal network, we used it to estimate the luminosity of the coronal network from the Fe IX/X brightness of the coronal network. We think that this estimate is accurate to order of

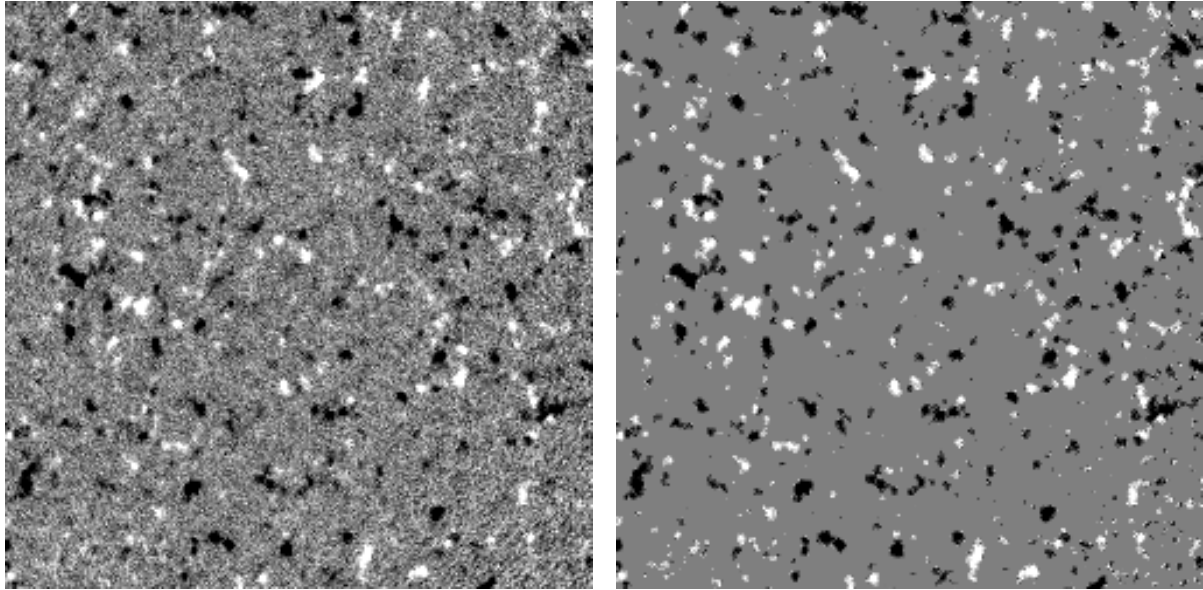


Figure 5 MDI magnetogram (left) in our example central square of quiet region shown in Figures 1-3, and the network magnetogram (right) extracted from this magnetogram.

magnitude, sufficiently accurate to show that the luminosity of the coronal network is nearly insignificant in comparison with the luminosity of the large-scale corona.

In Table 2, the area-average flux of coronal radiation from the $0.5 R_{\text{Sun}}$ central square is listed for the large-scale corona and for the coronal network. These values indicate that in quiet regions like ours the large-scale corona emits roughly 95% of the total coronal radiation, and that the corona in the central square had nearly the same average luminosity on all four days.

For comparison of the large-scale corona with the magnetic network in our quiet regions, we used a full-disk magnetogram taken by the Michelson Doppler Imager (MDI) on SOHO (Scherrer et al 1995) near the time of the coronal image each day. The times of our four magnetograms are listed in Table 1. These magnetograms are composed of square pixels, each 2.0 arcsec wide, and have a noise level of about 10 G. We registered each magnetogram with its corresponding coronal image by registering the solar limbs of the two full-disk images and then shifting the magnetogram to compensate for the solar rotation during the time between the two observations. In the $0.5 R_{\text{Sun}}$ central square, this procedure registered the magnetogram to the coronal image to within about the width of one pixel of the coronal image (2-3 arcsec). In the same way, the two coronal images for each day were registered to each other to this accuracy. As in Falconer et al (1998), the accuracy of the registration was verified by the coincidence of bright points in the pair of coronal network images with each other and with polarity dividing lines in the magnetogram. The first panel of Figure 5 shows the central square of the magnetogram for December 28. This magnetogram is registered to the central-square Fe IX/X coronal images shown in the previous Figures.

Because the magnetic field filling the large-scale corona is mainly rooted in the magnetic network lanes along the edges of the supergranules, in the present study we chose to examine the dependence of the luminosity (and hence the heating) of the large-scale corona on the magnetic flux content of the network lanes alone, in isolation from the so-called intranetwork magnetic field. The intranetwork magnetic flux is that in the interiors of the network cells (i.e., outside the

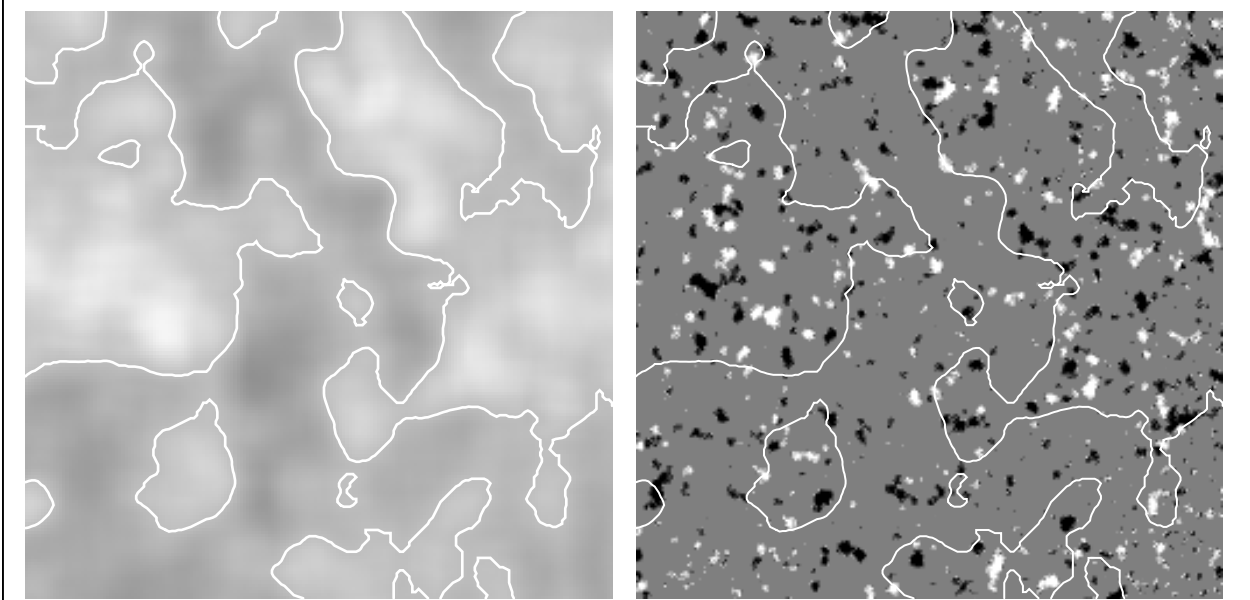


Figure 6 Bright and dim halves of the large-scale corona and their magnetic network in our example central quiet region. The white contour is the median brightness contour of the image of the large-scale corona from Figure 3. In the left panel, this contour is drawn on the image of the large-scale corona. In the right panel, the same contour is drawn on the network magnetogram of this region.

network lanes); it has a fine-scale mixture of both polarities, and is weaker than the network flux (Livingston & Harvey 1975; Wang & Zirin 1988; Martin 1988). We isolate the magnetic network flux from the intranetwork flux by extracting a network magnetogram from the total magnetogram by the following process, similar to the process used in Falconer et al (1998) to extract a polarity map of the magnetic network. First, the absolute (polarity-independent) magnetic flux in the total magnetogram is smoothed by a 3x3 pixel boxcar running average. Then, those pixels that have smoothed flux less than 7 G are masked out in the unsmoothed total magnetogram, leaving a magnetogram of the network alone. In this network magnetogram, the full spatial resolution, magnetic sensitivity, and magnetic polarity of the total magnetogram are retained in the unmasked areas, while the magnetic flux is set to zero in the masked areas. Effectively, the unmasked pixels constitute the lanes of the magnetic network, whereas the masked pixels cover the cell interiors. In Figure 5, the second panel shows the network magnetogram extracted from the MDI magnetogram in the first panel by this process. In each of our four central square quiet regions, the area occupied by network magnetic flux (the unmasked area) was about 10% of the total area.

In Table 2, the absolute magnetic flux content of the network magnetogram, per unit area of the entire $0.5 R_{\text{Sun}}$ central square, is listed for each of the four days. This shows that the network flux in the central square was roughly constant (fluctuated within a range of 15 %) over the four days.

We are now ready to address the following two specific questions. First, among subregions of our $0.5 R_{\text{Sun}}$ central square, does the luminosity of the large-scale corona increase with increasing magnetic flux in the underlying network? Second, if so, how strongly does the luminosity depend on the network flux; what is the steepness of the increase? From only visual comparison of the large-scale corona in the first panel of Figure 3 and its underlying magnetic network (second panel of Figure 5), it is not obvious at a glance whether the two have any

Date (Dec 1996)	Radiation Flux ($10^5 \text{ erg cm}^{-2} \text{ s}^{-1}$)		Network Mag. Flux (Gauss)		Network Flux Coast Length (10^6 km)	
	Dim Half	Brt. Half	Dim Half	Bright Half	Dim Half	Bright Half
27	0.93	1.2	1.3	2.7	5.2	6.8
28	0.97	1.3	1.2	3.3	5.2	8.0
29	0.96	1.3	1.5	2.9	5.9	6.9
30	0.95	1.3	1.6	3.1	5.8	7.0
Average:	0.95	1.3	1.4	3.0	5.5	7.2

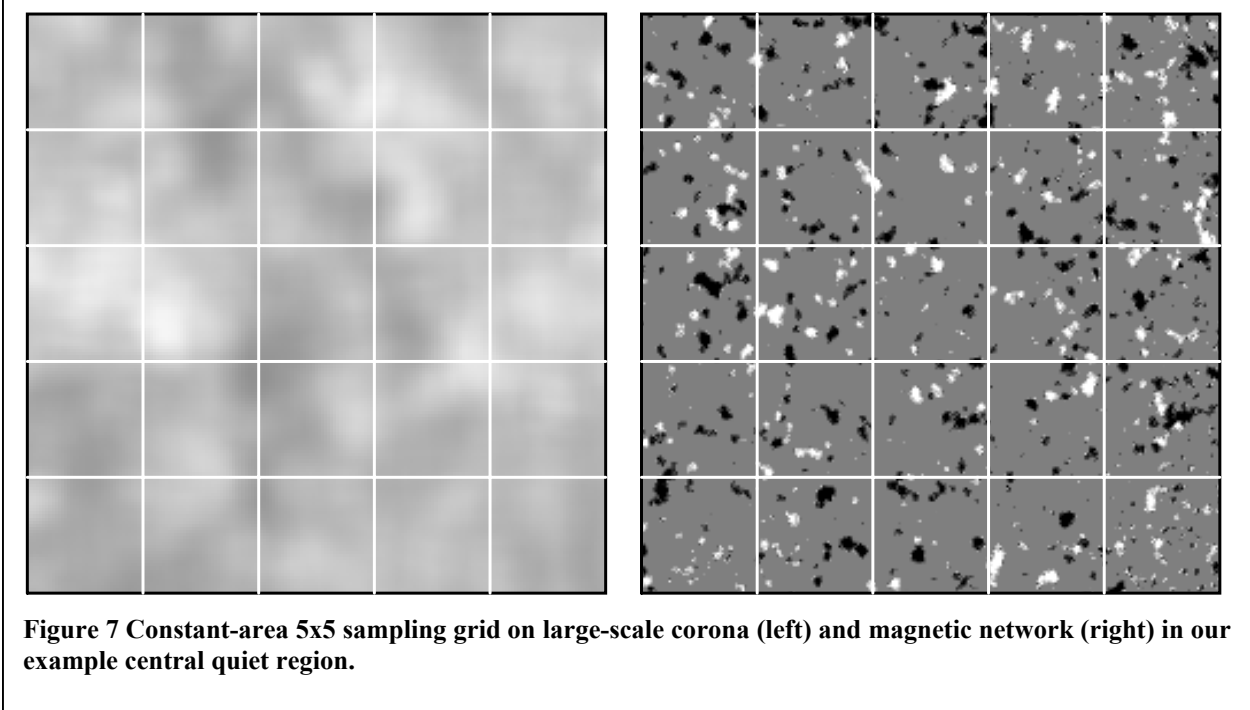
significant correlation. Definite answers to our two questions can be obtained only from measuring the luminosity of the large-scale corona in subregions and measuring the magnetic flux content of the network in the same subregions.

3. BRIGHT AND DIM HALVES OF THE LARGE-SCALE CORONA

By comparing the brighter half of the large-scale corona with the dimmer half, we can demonstrate that the luminosity of the large-scale corona definitely increases with network magnetic flux. In the first panel of Figure 6, the image of the large-scale corona from Figure 3 is shown with its median brightness contour. By definition, the median brightness contour divides the area of our central square in half. Moreover, the median contour makes it easy to see a characteristic of the large-scale corona: the large-scale corona is composed of bright “continents” and dark “oceans” having widths mostly in the range of 2-4 supergranules ($\sim 100,000 \text{ km}$) (Falconer et al 1999). In Table 3, the area-average radiation fluxes of the bright and dim halves of the large-scale corona are listed for each of the four days. On all four days, the bright half was about 40% more luminous than the dim half.

In the second panel of Figure 6, the median brightness contour from the first panel is superposed on the network magnetogram of the same region, the $0.5 R_{\text{Sun}}$ central square on December 28. From visual inspection of Figure 6, there appears to be more network magnetic flux under the bright half of the large-scale corona than under the dim half. In Table 3, the measured values of magnetic flux in the two halves of this network magnetogram (December 28) verify that there is more flux in the bright half than in the dim half, 2.8 times more. Table 3 shows that the network magnetic flux in the bright half exceeded that in the dim half by a similar amount on all four days. Averaged over the four days, there was 2.2 times more network flux in the bright half than in the dim half.

The measured values of large-scale coronal radiation flux and network magnetic flux in Table 3 establish that the luminosity of the large-scale corona does increase with the magnetic flux content of the underlying network. Table 3 also shows that the factor of increase from dim half to bright half is smaller for the luminosity than for the network magnetic flux. For the four-day average, the luminosity increases by a factor of 1.4 while the network flux increases by a factor of 2.2. These numbers suggest that the luminosity of the large-scale corona increases roughly as the square root of the magnetic flux content of the network. As the luminosity of the large-scale corona increases by a small amount ($< \sim 40\%$), the fraction of the heating energy

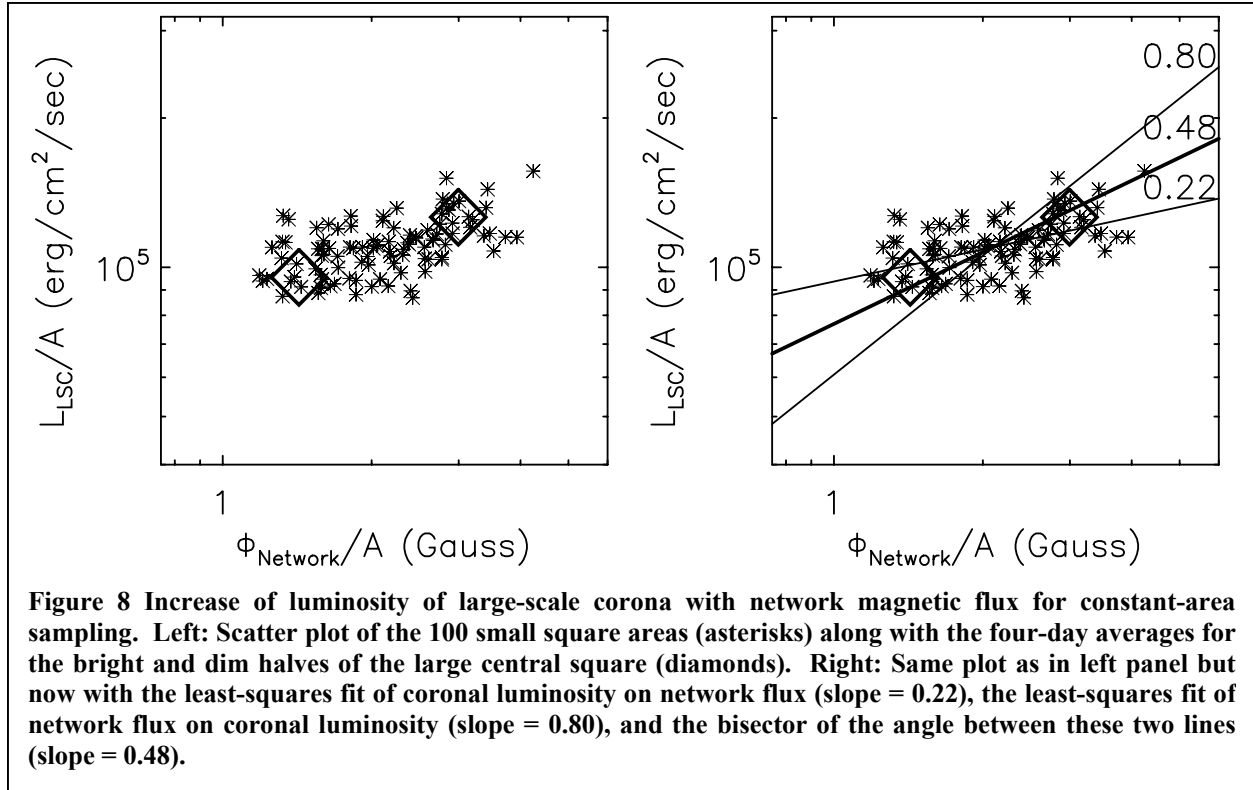


input going to the radiation output plausibly remains nearly constant, and the heating increases nearly in proportion to the luminosity. To this extent, a square-root scaling of luminosity with network flux content would indicate that the heating of the large-scale corona also increases roughly as the square root of the network flux content.

4. STEEPNESS OF THE INCREASE OF LUMINOSITY WITH NETWORK FLUX

We further examine the dependence of the large-scale coronal luminosity on the magnetic flux content of the network by measuring these quantities in many smaller equal-area regions within our four large central quiet regions. For this, we divide each of our large squares into a 5x5 grid of 25 small squares, as shown in Figure 7. Each small square is 70,000 km ($0.1 R_{\text{Sun}}$) wide, and so covers the area of about four supergranules. A small square is large enough that the large-scale corona above it should be magnetically rooted mostly in that square (e.g., see Dowdy et al 1986). This constant-area sampling of our four large regions gives 100 comparable pairs of measured values of large-scale coronal luminosity and network magnetic flux content.

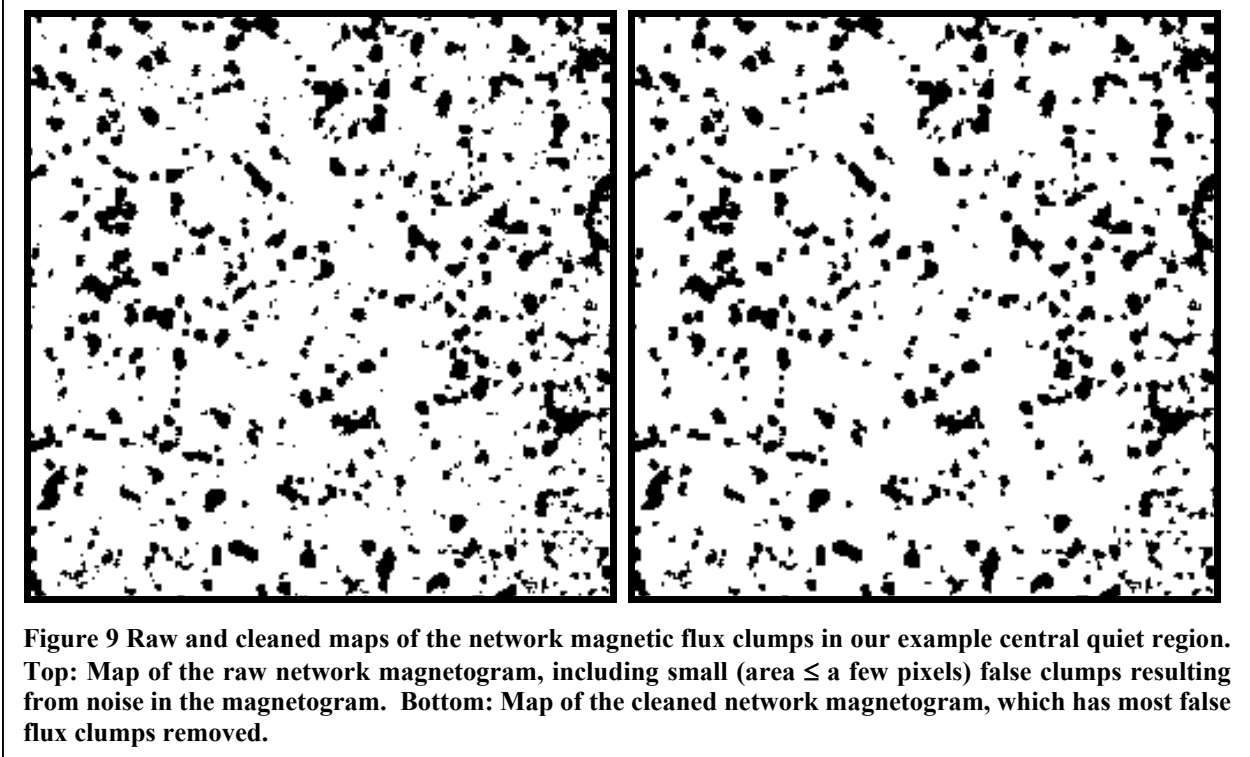
The Log-Log plot of luminosity versus network flux content (both normalized to unit area) for the 100 small squares is shown in the first panel of Figure 8. The 100 points form an elongated cloud along a trend of positive slope, luminosity increasing with network flux. The plot also includes two other points, shown as diamonds. The upper diamond marks the four-day average point for the bright half of the large-scale corona, the lower diamond the corresponding point for the dim half. It appears that the trend of the 100-point cloud is roughly the straight line defined by the two diamonds, which has a slope of 0.41. That is, the cloud of points from the 100 small squares appears to corroborate the indication from the bright and dim halves that the luminosity of the large-scale corona increases roughly as the square root of the magnetic flux content of the network (i.e., appears to have a trend slope in the vicinity of 0.5).



In Figure 8, the scatter of the 100 points about the trend is real, resulting from the complexity of the magnetic field and its activity, not from measurement error. The vertical and horizontal error bars of these data points, from noise in the Fe IX/X and Fe XII images of the large-scale corona and in the network magnetograms, are insignificant, smaller than the asterisks marking the points. We consider the physical scatter in the points to be both vertical (in luminosity) and horizontal (in network flux) because of the complex and random nature of the network magnetic flux distribution, of magnetic activity in the network, and of the linkage of the network flux in a small square to the large-scale corona above that square and adjacent squares. For these reasons, we expect that the luminosity should vary appreciably among squares having equal network magnetic flux content, and conversely that the network flux content should vary appreciably among squares having equal luminosity. On this basis, we assume that the breadth of the 100-point cloud about its major axis results from inherent scatter of the points in y (luminosity) and in x (network flux).

In cases such as ours, in which the points of a cloud of measured points (x,y) have scatter in both x and y , the slope of the least squares linear regression of y on x is an underestimate of the slope of the trend followed by the cloud. A better estimate of the trend slope can be found by combining the slope of the regression of y on x (which underestimates the trend slope) and the slope of the regression of x on y [which overestimates the trend slope (with respect to the x axis)] (e.g., Porter et al 1995). A standard estimate of the trend slope from these two slopes is the slope of the bisector, the slope of the line that bisects the angle between the two regression lines (Isobe et al 1990).

The second panel of Figure 8 shows the y on x regression line for the 100 points, the x on y regression line, and the bisector of the angle between the two regression lines. The slopes of the two regression lines are 0.22 and 0.80, giving the bisector line a slope of 0.48. This is consistent



with the luminosity of the large-scale corona increasing, on average, in proportion to the square root of the magnetic flux content of the network.

5. INCREASE OF LUMINOSITY WITH NETWORK FLUX COASTLINE LENGTH

That the luminosity of the large-scale corona increases roughly in proportion to the square root of the magnetic flux content of the network indicates that the heating of the large-scale corona is roughly proportional to the square root of the magnetic flux content of the network. Why should the heating of the body of the corona in quiet regions have this particular scaling with the network flux content? One possibility that comes to mind is the following. In Figure 6, while the magnetic network under the bright half of the large-scale corona and that under the dim half appear to be similar to each other in structure, the bright-half network flux clearly occupies more area than does the dim-half network flux. This suggests that the flux content of the network is roughly proportional to the area of the network flux, and hence that the heating of the large-scale corona is roughly proportional to the square root of the area occupied by the network flux in the photosphere. This, in turn, suggests that the heating increases roughly in proportion to the length of the perimeter (the “coastline”) of the network flux clumps. If so, this could mean that the heating of the large-scale corona is mainly driven by fine-scale magnetic activity along the edges of the network flux clumps: the greater the length of coastline, the greater the total amount of driving activity and coronal heating.

To test the above idea, we have measured the network flux coast length under the bright and dim halves of the large-scale corona. The first panel of Figure 9 is a map of the area occupied by the network magnetic flux in the network magnetogram shown in Figure 5. The network magnetogram retains the full signal of the MDI magnetogram in each unmasked pixel. Thus, the network magnetogram retains any noise present in the unmasked areas of the MDI magnetogram.

Any flux clump that is likely due to noise should not be included in the measured network flux coast length. To exclude those flux clumps that are likely false, we include only those clumps that each have flux content greater than the flux needed in a single pixel to produce a 2σ detection in that pixel. That is, we exclude any flux clump (of any area ≥ 1 pixel) having a flux content of less than 20 G times the area of one MDI pixel [$20 \text{ G} \times (1.45 \times 10^8 \text{ cm})^2 = 4.2 \times 10^{17} \text{ Mx}$]. By removing from the network area map in the first panel of Figure 9 each flux clump that has flux content below this noise level, we obtain the cleaned network flux area map shown in the second panel of Figure 9. As can be seen by inspection, the cleaned map has practically none of the many single-pixel clumps present in the uncleaned map. A few of the 2-pixel and 3-pixel clumps are also cleaned out.

This cleaning procedure removed only 1.4% of the magnetic flux and 3.2% of the flux area from the uncleaned network magnetograms. Hence, the noise in the network magnetograms was not large enough to significantly affect our measurement (from the uncleaned network magnetograms) of the scaling of the luminosity of the large-scale corona with the flux content of the network.

For each of the four days, from the cleaned network flux area map of the central square, our measured values of the network flux coast length under the bright and dim halves of the large-scale corona are listed in Table 3. For each half, the network coast length was roughly constant (fluctuated within a range of 15%) over the four days. The four-day average of the coast length in the bright half was 1.3 (7.2/5.5) times that in the dim half. This ratio is fairly close to the corresponding bright-half/dim-half ratio of 1.4 (1.3/0.95) for the large-scale coronal luminosity. Thus, our measurements indicate that the heating of the large-scale corona is roughly proportional to the coast length of the underlying network magnetic flux.

6. INTERPRETATION

The basic intent of the work reported here was to empirically determine the scaling of coronal heating in quiet regions with the magnetic flux content of the network, and from that, to gain new insight to the heating process. This approach to investigating coronal heating in quiet regions is basically the same as that taken by Fisher et al (1998) in their investigation of coronal heating in active regions. In particular, they examined the scaling of coronal heating of entire active regions with magnetic flux content by measuring the magnetic flux content Φ and coronal luminosity L of a few hundred active regions. These measurements showed that the coronal luminosity (and hence the coronal heating) of active regions increases with their magnetic flux content somewhat more strongly than linearly: $L \propto \Phi^{1.2}$.

At first sight, it appears that the coronal heating in active regions scales with magnetic flux differently than does the coronal heating in quiet regions, since we have found that the coronal heating in quiet regions scales roughly as the square root of the magnetic flux content of the network. To the contrary, because the scaling found by Fisher et al for active regions comes from a sampling of coronal luminosity and magnetic flux that is fundamentally different than our sampling of coronal luminosity and magnetic flux in quiet regions, the two scalings cannot be directly compared (Golub 2001). Fisher et al measured and compared whole active regions, which ranged over a factor of 100 in area, whereas we have measured and compared quiet regions of equal area. To compare the scaling of coronal heating with magnetic flux in quiet regions with the scaling found by Fisher et al for active regions, we will have to carry out a random-area sampling of quiet regions over a wide range in area. We are presently doing this, and plan to report the results in a follow-on paper in collaboration with Fisher.

From full-disk corona X-ray images from the Yohkoh Soft X-ray Telescope (SXT) and full-disk magnetograms from the National Solar Observatory, Kitt Peak, Pevtsov & Acton (2001) have pointed out that the emergence of an active region in the middle of an otherwise quiet hemisphere of the Sun can result in enhanced coronal heating in surrounding quiet regions over much of the hemisphere, including some quiet regions that have no direct magnetic connection to the new active region. From Yohkoh SXT full-disk corona images and MDI full-disk magnetograms, Moore, Falconer, & Sterling (2001) have presented examples of such remote coronal heating occurring in response to the emergence of new magnetic flux in existing active regions, and have termed this effect “contagious coronal heating.” Both Pevtsov & Acton (2001) and Moore et al (2002) conclude that the remote enhanced coronal heating is triggered and/or driven by the active-region flux emergence and not driven by network activity in the remote quiet region. Thus, we must consider whether any significant amount of the coronal heating in our quiet regions was caused by remote active regions. For the following reasons, we believe that any such heating was negligible in our regions. During the four days of our observations of the central square of quiet region, (1) the full-disk coronal images from EIT and SXT showed evidence of only two active regions on the Sun, one going over the west limb and the other approaching the southeast limb from the far side, (2) the full-disk MDI magnetograms (from before, during, and after our four days) showed that these were old decayed active regions having no sunspots, and (3) neither the magnetograms nor the coronal images showed any evidence (of the type presented by Moore et al 2002) of new flux emergence in these active regions. Furthermore, as in Figure 1, the full-disk coronal images showed no indication that the coronal heating in the central square was affected by either of these very remote old active regions.

Our measurements show that the luminosity of the large-scale corona in our quiet regions is nearly proportional to the coast length of the underlying network magnetic flux in the photosphere. From this result, we infer that in the absence of influence from active regions the coronal heating in quiet regions is roughly proportional to the network flux coast length, and propose that the coronal heating in such quiet regions is mainly driven by fine-scale magnetic activity along the edges of the network flux clumps. This interpretation is encouraged by fine-scale eruptive events observed in the network in sequences of high-resolution images and imaged spectra of the chromosphere and transition region.

Many explosive events of the spatial scale of spicules and macropicules (1,000-10,000 km in width) are observed in imaged EUV line spectra of the lower transition region in quiet regions. These typically have velocities of ~ 100 km/s, lifetimes of ~ 60 s, and occur frequently enough that at any instant there are one or two in progress per supergranule (Dere, Bartoe, & Brueckner 1989). Porter and Dere (1991) examined the location of such explosive events relative to the photospheric magnetic flux clumps of the network. They found that most are located at the edges of flux clumps.

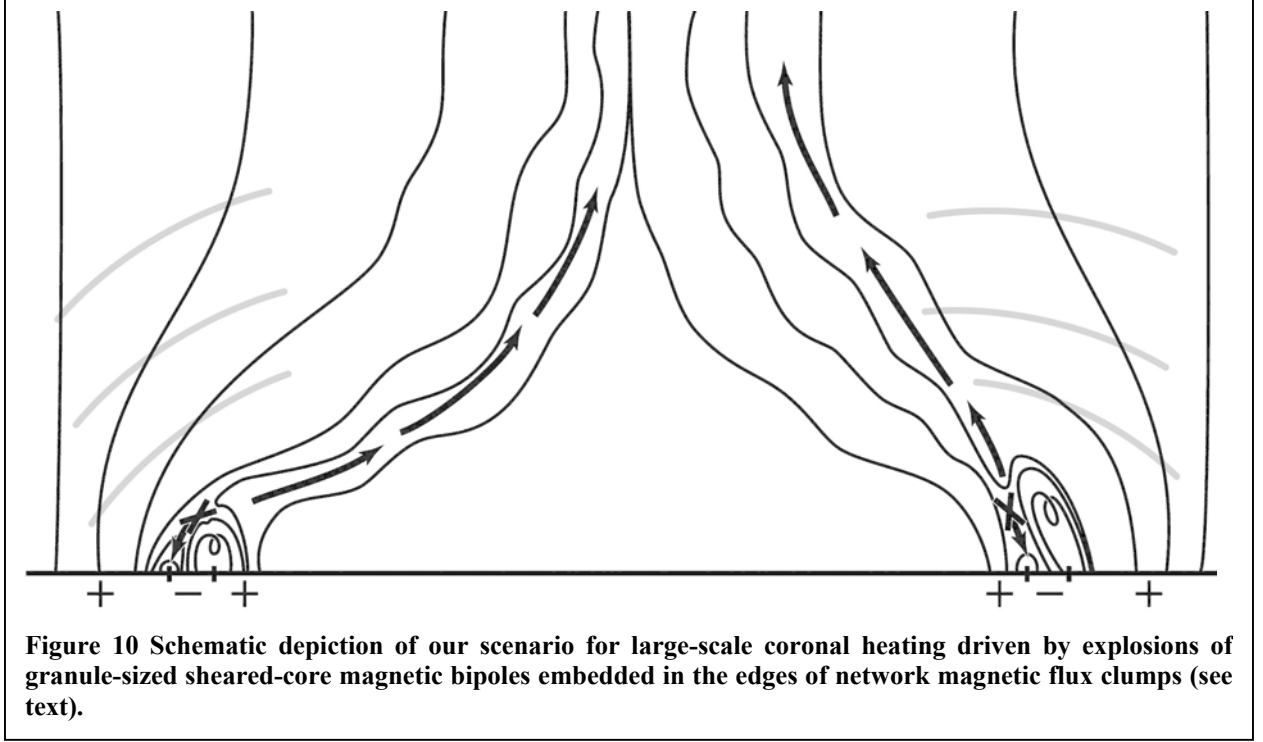
The above EUV explosive events may be the high-energy extreme of a larger population of fine-scale explosive events in the network, the majority of which produce chromospheric spicules. Spicules typically have widths $\leq 1,000$ km, velocities of ~ 25 km/s, heights $\geq 4,000$ km, and lifetimes of ~ 5 min (Lynch, Beckers, & Dunn 1973; Sterling 2000). Spicules occur so frequently that at any instant there are ~ 30 spicules present per supergranule (Beckers 1972; Lynch et al 1973). High-resolution $H\alpha$ filtergrams together with photospheric magnetograms show that most spicules, like the more energetic network explosive events, are rooted along the edges of network flux clumps (Beckers 1968; Dunn & Zirker 1973; Zirin 1988). Thus, the edges

of the network flux clumps are observed to be riddled with fine-scale explosive events. Our evidence that coronal heating in quiet regions increases in rough proportion to the network flux coast length suggests that the aggregate of these network edge events may be the main driver of the heating.

In previous work (Falconer et al 1997, 2000; Porter et al 1998), we have proposed that the coronal heating in active regions is mostly driven by microflaring activity in low-lying sheared core fields. (A sheared core field consists of low-arching field lines that encase a polarity dividing line and that are sheared across this line so that the opposite feet have offsets along the dividing line that are large relative to their offsets normal to the dividing line.) In Moore et al (1999), we showed that our idea of driving coronal heating in active regions by microexplosions of strands of sheared core field was energetically feasible in terms of the coronal heating rate and core magnetic field strength and shear observed in a real active region. We also pointed out that, because the magnetic network in quiet regions is riddled with polarity dividing lines, there might be enough miniature sheared core fields in the network for coronal heating in quiet regions to be mainly driven by explosions of these core fields. Our scenario for coronal heating in active regions by core-field microexplosions is depicted in Figure 5 of Moore et al (1999). In light of our evidence that coronal heating in quiet regions is nearly proportional to the network flux coast length, our corresponding scenario for coronal heating in quiet regions is as depicted in Figure 10.

Figure 10 depicts representative network magnetic field and network microflaring activity stemming from the edges of a supergranular network cell in and above the photosphere. These are shown in a vertical plane through the center of the cell. In this example field arrangement, the vertical plane cuts through two positive-polarity network field clumps that sit on opposite sides of the cell. These magnetic fields fan out with height to merge in the large-scale corona over the interior of the cell. Each of these two flux clumps has a small sheared-core bipole embedded near its edge. There is a magnetic null over the negative polarity of each of these bipoles. The sheared core field in each bipole is shown in the act of exploding upward and driving reconnection at the null (marked by an X). The reconnection generates upward and downward plasma jets and/or streams of energized particles (denoted by the arrows). The upward plasma jets might be manifested as $H\alpha$ spicules or EUV macrospicules. The core-field explosion and the reconnection also generate MHD waves (denoted by gray arcs and by wiggles in the field lines) that propagate up into the large-scale corona. The scenario suggested by our results is that the heating of the large-scale corona above the network cell is mainly driven via these disturbances by such explosions of small sheared-core bipoles in the network, and that most of these occur in the edges of the network flux clumps.

The topology of the magnetic field rooted in and around the embedded bipoles in Figure 10 is the same as that of the field rooted in and around the magnetic island in the active region depicted in Figure 5 of Moore et al (1999). Explosions of the core field on one side of the magnetic island drives coronal heating in the active region in the same ways that explosions of the core fields of the embedded bipoles in Figure 10 drive quiet-region coronal heating. This same field configuration, in which reconnection can be driven at the magnetic null between a bipole and surrounding unipolar field, has been proposed by Karpen, Antiochos, & DeVore (1996) for coronal heating in active regions and by Shibata for X-ray jets and $H\alpha$ surges (Shibata et al 1992; Shibata 1996, 1998, 1999). Given this field configuration, spicules, surges, and X-ray jets can all be produced in the same way: in each case plasma is jetted upward along those far-reaching field lines that have their feet shifted by the reconnection (as in Figure 10).



The scenario depicted in Figure 10 for quiet-region coronal heating can be shown to be energetically feasible by the following estimate of the number N of active sheared-core network bipoles that need to be present per supergranule to heat the corona. This number is given by

$$N = \dot{E}_{\text{corona}} / \dot{E}_{\text{SCNB}} \quad (1)$$

where \dot{E}_{corona} is the rate of energy input to coronal heating per supergranule, and \dot{E}_{SCNB} is the rate of energy output going to coronal heating from an average active sheared-core network bipole. The coronal heating rate per supergranule is

$$\dot{E}_{\text{corona}} = A_{\text{SG}} F_{\text{corona}} \approx 3 \times 10^{24} \text{ ergs/s}, \quad (2)$$

where A_{SG} is the area of a supergranule [$A_{\text{SG}} \approx (30,000 \text{ km})^2 \approx 10^{19} \text{ cm}^2$], and F_{corona} is the energy flux for coronal heating. For quiet regions, $F_{\text{corona}} \approx 3 \times 10^5 \text{ ergs cm}^{-2} \text{ s}^{-1}$ (Withbroe & Noyes 1977). The rate of coronal heating by an active sheared-core network bipole is given by

$$\dot{E}_{\text{SCNB}} \approx E_{\text{SCNB}} / \tau, \quad (3)$$

where E_{SCNB} is the free magnetic energy spent on coronal heating by an average active sheared-core network bipole during its life, and τ is the lifetime of the bipole. Thus, we have

$$N \approx 3 \times 10^{24} \tau / E_{\text{SCNB}}. \quad (4)$$

The coronal heating energy per active bipole is given by

$$E_{\text{SCNB}} = f E_{\text{explosion}}, \quad (5)$$

where $E_{\text{explosion}}$ is the energy released in the explosion of an average sheared-core network bipole, and f is the fraction of this energy that goes to coronal heating. We assume that our miniature sheared core field explosions are similar to the large sheared core field explosions in flares and coronal mass ejections. Then, following Moore (1988),

$$E_{\text{explosion}} \sim V_0 B_0^2 / 8\pi, \quad (6)$$

where V_0 is the initial volume of the exploding core-field flux rope and B_0 is the initial field strength in the flux rope. Taking the initial shape of the flux rope to be roughly cylindrical, the initial volume is approximated by

$$V_0 \sim \pi r_0^2 l_0, \quad (7)$$

where l_0 and r_0 are the initial length and radius of the flux rope. With these approximations, we have

$$N \sim 2.4 \times 10^{25} (l_0/r_0)^2 \tau l_0^{-3} f^1 B_0^{-2}. \quad (8)$$

If the initial aspect ratio l_0/r_0 of the exploding flux rope is similar to that in eruptive flares, then from Moore (1988), $l_0/r_0 \sim 10$. If a typical network sheared core field explosion produces a spicule, then because spicules have widths of the order of those of photospheric granules, it is reasonable to expect these exploding network bipoles to have widths and lifetimes comparable to those of the granules. It might be that these bipoles are generated and destroyed by the granular convection churning the magnetic field at the edges of the network flux clumps. Taking the observed average granule size and lifetime found by Title et al (1989), we have $l_0 \sim 10^8$ cm and $\tau \sim 300$ s. These values of l_0/r_0 , l_0 , and τ give

$$N \sim 7 \times 10^5 f^1 B_0^{-2}. \quad (9)$$

If, say, roughly a quarter of the energy of each explosion goes into coronal heating ($f \sim 1/4$), then for an initial field strength of order 300 G in the exploding sheared core field, we obtain $N \sim 30$ for the number of active sheared-core bipoles required to be present per supergranule in order to heat the corona. It is gratifying that the observed number of spicules present per supergranule is also ~ 30 (Lynch et al 1973). So, if such small, strong, active sheared-core bipoles are present in such numbers in the edges of the network flux clumps, then it is energetically entirely feasible for these micro magnetic explosions to be the main drivers of the heating of the overlying large-scale corona in the manner depicted in Figure 10.

The active sheared-core network bipoles that we posit have magnetic flux of each polarity of $\sim 10^{18}$ Mx. If either polarity were isolated in a single MDI pixel it would be detectable. However, because the spatial resolution is only 4 arcsec for the MDI full-disk magnetograms and 1.25 arcsec ($\approx 10^8$ cm) for the MDI high-resolution mode, our bipoles would be hardly detectable if at all in MDI magnetograms. We look forward to the vector magnetograms from the forthcoming Japan/US/UK Solar-B mission, to be launched in 2005. The Solar-B magnetograms

are to have spatial resolution of 0.25 arcsec (1.8×10^7 km), a transverse field sensitivity of ~ 100 G, and a line-of-sight field sensitivity of ~ 10 G.

In view of our observational results and their interpretation presented in this paper, we predict that (1) transient sheared-core bipoles of the size of granules and having transverse field strengths $> \sim 100$ G will be found at the edges of network flux clumps, (2) ~ 30 of these bipoles will be found present per supergranule, and (3) most spicules will be found to come from explosions of these bipoles.

From physical reasoning and from modeling of observed properties of the fast solar wind from coronal holes, Axford and McKenzie have long contended (1) that the corona and solar wind in and from coronal holes are heated and accelerated by high-frequency MHD waves having periods $< \sim 1$ s, (2) that these waves are generated by fine-scale reconnection events (microflares) low in the magnetic network, and (3) that such microflaring activity in the network drives the heating of the corona in quiet regions that are not in coronal holes (Axford & McKenzie 1992, 1997; Axford et al 1999). Our observational results bolster this view, and our scenario for quiet-region coronal heating amounts to a variation of the picture advocated by Axford and McKenzie. The essential ingredient is the mixture of magnetic fluxes of opposite polarity on granular and subgranular scales in the magnetic network. It remains to be observed [by Solar-B and/or by large ground-based solar telescopes equipped with adaptive optics (Parker et al 1998; Knoelker et al 2001)] whether, where, and how opposite polarities are mixed on these scales in the network.

This work was supported by NASA's Office of Space Science through its Solar and Heliospheric Physics Supporting Research and Technology Program and its Sun-Earth Connection Guest Investigator Program. We thank Leon Golub for pointing out to us that the scaling that we have found between coronal luminosity and network magnetic flux content in quiet regions cannot be directly compared to the scaling found by Fisher et al (1998) between the coronal luminosity and magnetic flux content of active regions. Comments from the referee resulted in a better presentation of the method of measuring the coronal luminosity, and of the rationale for its validity.

REFERENCES

- Acton, L. W. 1996, in *Magnetohydrodynamic Phenomena in the Solar Atmosphere – Prototypes of Stellar Magnetic Activity*, ed. Y. Uchida, T. Kosugi, & H. S. Hudson (Dordrecht: Kluwer), 3.
- Acton, L., Tsuneta, S., Ogawara, Y. et al 1992, *Science*, 258, 618.
- Allen, C. W. 1973, *Astrophysical Quantities* (London: Athlone), 181.
- Axford, W. I., & McKenzie, J. F. 1992, in *Solar Wind Seven*, ed. E. Marsch & R. Schwenn (Oxford: Pergamon), 1.
- Axford, W. I., & McKenzie, J. F. 1997, in *Cosmic Winds and the Heliosphere*, ed. J. R. Jokipii, C. P. Sonett, & M. S. Giampapa (Tucson: University of Arizona Press), 31.
- Axford, W. I., McKenzie, J. F., Sukhorukova, G. V., Banaszekiewicz, M., Czechowski, A., & Ratkiewicz, R. 1999, *Space Sci. Rev.*, 87, 25.
- Beckers, J. M. 1968, *Sol. Phys.*, 3, 367.
- Beckers, J. M. 1972, *ARA&A*, 10, 73.
- Cook, J. W., Cheng, C.-C., Jacobs, V. L., & Antiochos, S. K. 1989, *ApJ*, 338, 1176.

- Cranmer, S. R. 2002, in *Multi-Wavelength Observations of Coronal Structure and Dynamics*, ed. P. C. H. Martens & D. P. Cauffman (Amsterdam: Pergamon), 3.
- Delaboudiniere, J.-P., et al 1995, *Sol. Phys.*, 162, 291.
- Dere, K. P., Bartoe, J.-D. F., & Bueckner, G. E. 1989, *Sol. Phys.*, 123, 41.
- Dere, K. P., Landi, E., Mason, H. E., Monsignori Fossi, B. C., & Young, P. R. 1997, *A&A Suppl.*, 125, 149.
- Dowdy, J. F., Jr., Rabin, D., & Moore, R. L. 1986, *Sol. Phys.*, 105, 35.
- Dunn, R. B., & Zirker, J. B. 1973, *Sol. Phys.*, 33, 281.
- Falconer, D. A., Gary, G. A., Moore, R. L., & Porter, J. G. 2000, *ApJ*, 528, 1004.
- Falconer, D. A., Moore, R. L., Porter, J. G., Gary, G. A., & Shimizu, T. 1997, *ApJ*, 482, 519.
- Falconer, D. A., Moore, R. L., Porter, J. G., & Hathaway, D. H. 1998, *ApJ*, 501, 386.
- Falconer, D. A., Moore, R. L., Porter, J. G., & Hathaway, D. H. 1999, *Space Sci. Rev.*, 87, 181.
- Fisher, G. H., Longcope, D. W., Metcalf, T. R., & Pevtsov, A. A. 1998, *ApJ*, 508, 885.
- Foley, C. R., Culhane, J. L., Acton, L. W., & Lemen, J. R. 1992, in *Magnetohydrodynamic Phenomena in the Solar Atmosphere – Prototypes of Stellar Magnetic Activity*, ed. Y. Uchida, T. Kosugi, & H. S. Hudson (Dordrecht: Kluwer), 565.
- Golub, L. 2001, private communication.
- Harvey-Angle, K. L. 1993, *Magnetic Bipoles on the Sun*, PhD Dissertation (Utrecht: Utrecht University), 304.
- Isobe, T., Feigelson, E. D., Akritas, M. G., & Babu, G. J. 1990, *ApJ*, 364, 104.
- Karpen, J. T., Antiochos, S. K., & DeVore, C. R. 1996, *ApJ*, 460, L73.
- Knoelker, M., et al 2001, in *Astronomy and Astrophysics in the New Millennium: Panel Reports* (Washington, DC: National Academy Press), 221.
- Leighton, R. B. 1963, *ARA&A*, 1, 19.
- Livingston, W. C., & Harvey, J. 1975, *BAAS*, 7, 346.
- Lynch, D. K., Beckers, J. M., & Dunn, R. B. 1973, *Sol. Phys.*, 30, 63.
- Martens, P. C. H., Cirtain, J. W., & Schmelz, J. T. 2002, *ApJ*, 577, L115.
- Martin, S. F. 1988, *Sol. Phys.*, 117, 243.
- Moore, R. L. 1988, *ApJ*, 324, 1132.
- Moore, R. L., Falconer, D. A., Porter, J. G., & Suess, S. T. 1999, *ApJ*, 526, 505.
- Moore, R. L., Falconer, D. A., & Sterling, A. C. 2002, in *Multi-Wavelength Observations of Coronal Structure and Dynamics*, ed. P. C. H. Martens & D. P. Cauffman (Amsterdam: Pergamon), 39.
- Moore, R. L., Musielak, Z. E., Suess, S. T., & An, C.-H. 1991, *ApJ*, 378, 347.
- Parker, E. N. 1963, *Interplanetary Dynamical Processes* (New York: Wiley).
- Parker, E. N. 1983, *ApJ*, 264, 642.
- Parker, E. N. 1987, *Physics Today*, 40(7), 36.
- Parker, E. N. 1991, *ApJ*, 372, 719.
- Parker, E. N., et al 1998, *Ground-Based Solar Research: An Assessment and Strategy for the Future* (Washington, DC: National Academy Press).
- Pevtsov, A. A., & Acton, L. W. 2001, *ApJ*, 554, 416.
- Porter, J. G., & Dere, K. P. 1991, *ApJ*, 370, 775.
- Porter, J. G., Falconer, D. A., & Moore, R. L. 1998, in *Solar Jets and Coronal Plumes*, ed. T.-D. Guyenne (ESA-SP421; Noordwijk, ESA), 147.
- Porter, J. G., Fontenla, J. M., & Simnett, G. M. 1995, *ApJ*, 438, 472.

- Porter, J. G., & Moore, R. L. 1988, in *Solar and Stellar Coronal Structure and Dynamics*, ed. R. C. Altrick (Sunspot, New Mexico: National Solar Observatory, Sacramento Peak), 125.
- Porter, J. G., Moore, R. L., Reichmann, E. J., Engvold, O., & Harvey, K. L. 1987, *ApJ*, 323, 775.
- Scherrer, P. H., et al 1995, *Sol. Phys.*, 162, 129.
- Schrijver, C. J., Title, A. M., et al 1999, *Sol. Phys.*, 187, 261.
- Schmelz, J. T. 2002, *ApJ*, 578, L161.
- Schmelz, J. T., Scopes, R. T., Cirtain, J. W., Winter, H. D., & Allen, J. D. 2001, *ApJ*, 556, 896.
- Sheeley, N. R., Jr. 1992, in *The Astronomy and Astrophysics Encyclopedia*, ed. S. P. Maran (New York: Van Nostrand), 854.
- Shibata, K. 1996, in *Magnetohydrodynamic Phenomena in the Solar Atmosphere – Prototypes of Stellar Magnetic Activity*, ed. Y. Uchida, T. Kosugi, & H. S. Hudson (Dordrecht: Kluwer), 13.
- Shibata, K. 1998, in *Observational Plasma Astrophysics: Five Years of Yohkoh and Beyond*, ed. T. Watanabe, T. Kosugi, & A. C. Sterling (Dordrecht: Kluwer), 187.
- Shibata, K. 1999, *Astrophys. and Space Sci.*, 264, 129.
- Shibata, K., et al 1992, *PASJ*, 44, L173.
- Sterling, A. C. 2000, *Sol. Phys.*, 196, 79.
- Title, A. M., Tarbell, T. D., Topka, K. P., Ferguson, S. H., Shine, R. A., & The SOUP Team 1989, *ApJ*, 336, 475.
- Vaiana, G. S., & Rosner, R. 1978, *ARA&A*, 16, 393.
- Wang, H., & Zirin, H. 1988, *Sol. Phys.*, 115, 205.
- Withbroe, G. L. 1988, *ApJ*, 325, 442.
- Withbroe, G. L. 1992, in *The Astronomy and Astrophysics Encyclopedia*, ed. S. P. Maran (New York: Van Nostrand), 858.
- Withbroe, G. L. & Noyes, R. W. 1977, *ARA&A*, 15, 363.
- Zirin, H. 1988, *Astrophysics of the Sun* (Cambridge: Cambridge University Press), Chapter 7, 155.